Contribution from the Department of Chemistry,
The University of Chicago, Chicago, Illinois 60637

Geometrical and Electronic Links among the Structures of MX_2 Solids: Structural Enumeration and Electronic Stability of Pyrite-like Systems

JEREMY K. BURDETT*[1] and TIMOTHY J. McLARNAN

Received July 9, 1981

Adding valence electrons to 10-electron systems with the CaC_2 structure results in MX_2 structures such as those of pyrite and marcasite, which are obtained from CaC_2 by rotating the X_2 units away from 001. Band structure calculations using the extended Hückel approach attribute this effect to stabilization of dimer π_g^* orbitals on distortion, an analysis parallel to the traditional orbital explanation for the molecular conformations of C_2F_2, N_2F_2, and O_2F_2. Of the nine structures having the same size unit cells as pyrite and derived from CaC_2 in this way, the three observed types (pyrite, marcasite, and $NaHF_2$) lie lowest in energy. The others are destabilized by dimer–dimer repulsions. The distortion of the MX_6 octahedra found in löllingite ($FeAs_2$) is correctly predicted to occur for d^4 metals but not for d^6 ones. It is also shown how several common structures of MX_2 systems can be derived from one another geometrically and how these geometric derivations relate to the number of valence electrons.

Introduction

There are from a philosophic point of view two general approaches to the theoretical study of the equilibrium geometries of molecules and crystals. The first is to develop increasingly elaborate mathematical methods for solving the wave equation and to apply these—generally to small molecules—with an eye to achieving greater and greater numerical accuracy. The ultimate goal of this program would be an algorithm capable of calculating molecular or crystal properties as accurately as desired and possibly more easily and less expensively than these properties could be measured. The alternative approach, which we shall employ here, seeks instead to use approximate calculations to obtain simple semiquantitative rules based on such notions as symmetry, electronegativity, and overlap that rationalize observed geometries and properties. Ultimately, this project might hope to produce an understanding of structure in which a "back of the envelope" calculation could be performed to give a rough prediction which would usually be right and which could, if desired, be backed up by accurate computations. This development and codification of intuitions are of considerable use in cases where accurate numerical solutions are impossible, and may provide a type of understanding that such computations often bury within the machine. Of course, it may also at times give the wrong answer, but from these cases there is generally something to be learned as well.

In applying either of these methods to the geometries of a family of structurally related molecules or crystals, it is often extremely helpful to develop a description of the structures that permits the enumeration of all such possible configurations, real and hypothetical, derived from a parent in some specific way. This provides an objective basis on which to test the ability of good calculations to predict the correct atomic arrangement. It may suggest what factors stabilize the observed types over those which are unobserved so that we may hazard predictions as to likely configurations not yet observed. We have previously used the approach of enumeration followed by analysis using extended Hückel based band structure calculations to study a set of structures related to those of arsenic and black phosphorus.[2a] These can be derived from the NaCl or simple cubic structure as a result of the Gedanken process of adding additional valence electrons to antibonding orbitals and then breaking bonds around each center. The resulting understanding of these particular structures grows naturally from molecular orbital ideas traditionally used to rationalize molecular geometries and is compatible with the geometries and electronic structures of finite clusters of atoms that retain the local geometric environment of the solid.

Genealogy of Structures

Bond breaking (as in the rock salt → arsenic system described above) is not the only way a structure can respond to addition of electrons to high-energy orbitals. Consider the 22-e molecule C_2F_2 (**1**). As electrons are added to this molecule,

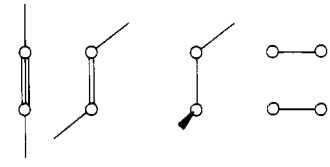

1 2 3 4

it suffers progressive bending to assume the geometries of N_2F_2 (**2**) (24 e) and O_2F_2 (**3**) (26 e) before the central linkage is finally broken in $2F_2$ (**4**) (28 e). A similar sequence is observed in C_2H_2 (10 e), N_2H_2 (12 e), O_2H_2 (14 e), and 2HF (16 e), except that the equilibrium geometry of N_2H_2 is nonplanar.

The same phenomenon can be seen in the solid-state structures of CaC_2, pyrite (FeS_2), and CaF_2, which form the basis for the present study.[2b] The CaC_2 type (Figure 1) with 10 valence electrons is obtained from the NaCl structure by replacing Na with Ca and Cl with C_2 dimers oriented along the 001 crystallographic direction. In the 14-e pyrite structure (Figure 2), the dimers have rotated to a bent geometry, from which the 16-e CaF_2 structure (Figure 3) can be derived by breaking the X_2 dimers and moving these atoms apart. With still more electrons, one finds the 22-e XeF_2 type (Figure 4), which can be obtained from CaF_2 by moving the metal atoms to the centers of the edges of the MX_8 coordination cubes, thereby breaking M–X bonds.

In these and the following drawings of structures, we have often followed crystal chemists' tradition by showing not the bonds from an atom to its neighbors but the edges of the resulting coordination polyhedron. Thus, an octahedral MX_6 unit may be given any of the representations shown in **5**, depending on its orientation.

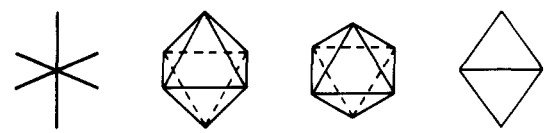

5

(1) Fellow of the Alfred P. Sloan Foundation and Camille and Henry Dreyfus Teacher Scholar.

(2) (a) Burdett, J. K.; McLarnan, T. J.; Haaland, P. *J. Chem. Phys.* **1981**, *75*, 5774. (b) All crystal structures are taken from: Wyckoff, R. W. G. "Crystal Structures", 2nd ed.; Wiley-Interscience: New York, 1963. Pearson, W. B. "The Crystal Chemistry and Physics of Metals and Alloys"; Wiley-Interscience: New York, 1972. Wells, A. F. "Structural Inorganic Chemistry", 4th ed.; Oxford University Press: London, 1975. (c) Hulliger, E. *Struct. Bonding (Berlin)* **1968**, *4*, 83.

0020-1669/82/1321-1119$01.25/0

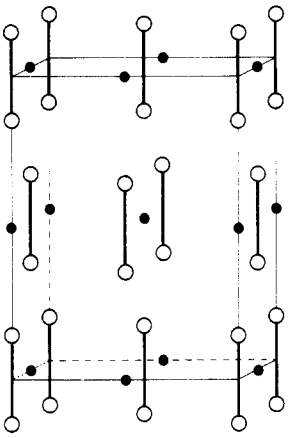

Figure 1. CaC_2 structure. Filled circles represent Ca atoms and open circles represent C atoms. The unit cell shown is double the conventional cell.

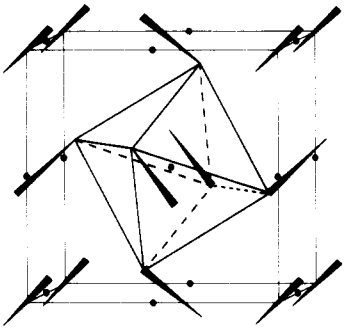

Figure 2. Pyrite structure. Small filled circles represent Fe atoms andd narrow wedges represent S_2 dimers, with the atom at the broad end nearer the reader than the atom at the pointed end. Each of these dimers points in a direction parallel to one of the body diagonals of the cubic unit cell shown. The coordination octahedron of the central Fe atom is also shown.

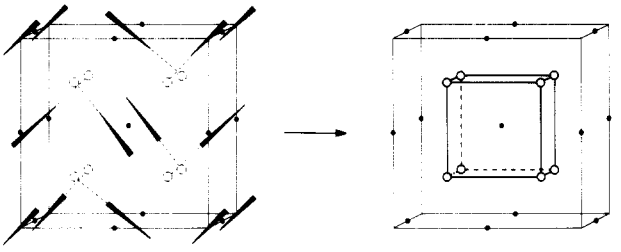

Figure 3. Derivation of the CaF_2 structure (right) from the pyrite structure. In this derivation, the dimers are broken, i.e., the anions connected by S–S bonds in pyrite move directly away from one another. Only the tracks of the dimer atoms within the given unit cell are shown. The resulting cubic coordination of the central metal atom is shown.

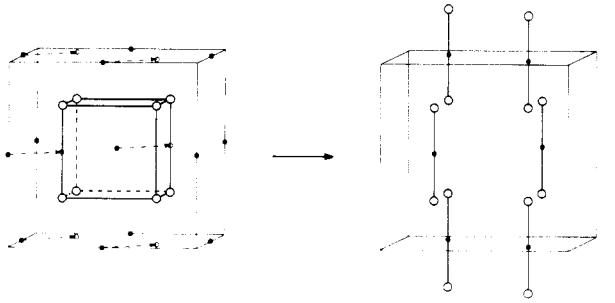

Figure 4. Derivation of the XeF_2 structure (right) from the CaF_2 structure. In this derivation, metal–anion bonds are broken so that metal atoms move to the edges of their former coordination cubes. The resulting structure is a packing of linear F–Xe–F units.

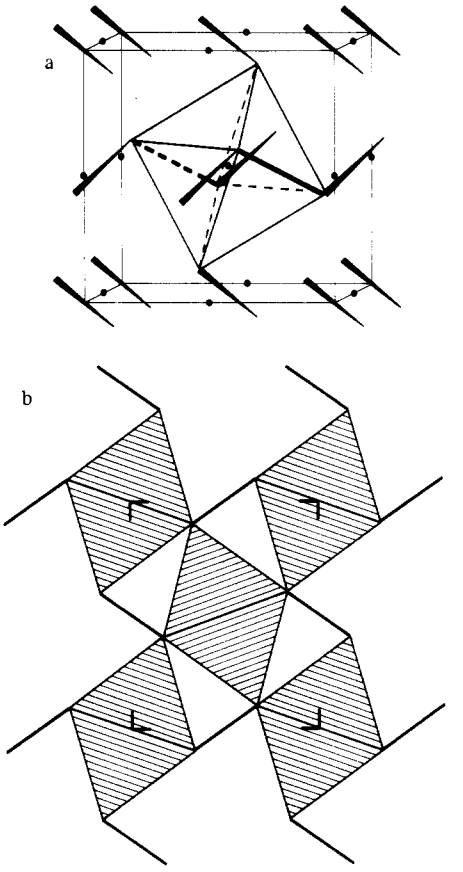

Figure 5. (a) Marcasite structure, shown with the conventions of Figure 2. The two heavy edges of the coordination octahedron shown are shared with other octahedra to form infinite chains along the 110 direction of the cubic cell shown, which is in fact double the conventional cell. (b) Arrangement of these octahedra viewed down the infinite chains. The octahedra are shaded and the S–S dimers are shown as heavy lines. The conventional unit cell is indicated.

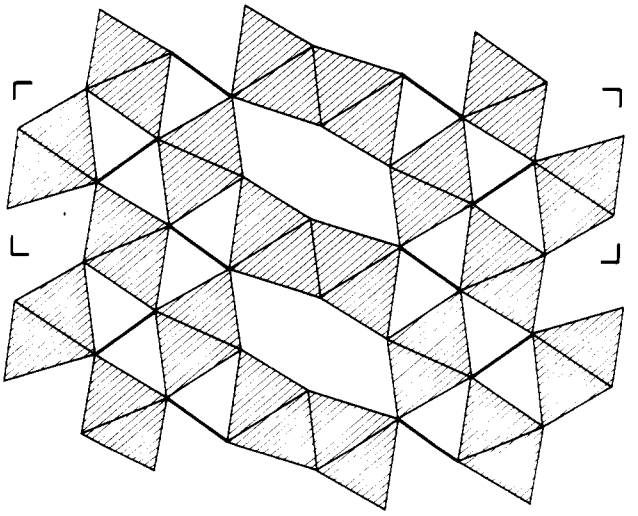

Figure 6. Observed atomic positions in the $IrSe_2$ structure, seen down infinite chains of octahedra like those of marcasite. This structure contains marcasite-like slabs containing Se–Se bonds and slabs containing edge-sharing octahedra in which such bonds have been broken.

Alternatively, rotation of the dimers in CaC_2 in a different manner followed by a little distortion produces the structure of marcasite (Figure 5), another polymorph of FeS_2. Adding more electrons produces the 15-e $IrSe_2$ structure (Figure 6), which has half of the marcasite dimer bonds broken, and eventually the 16-e rutile (TiO_2) structure (Figure 7), in which

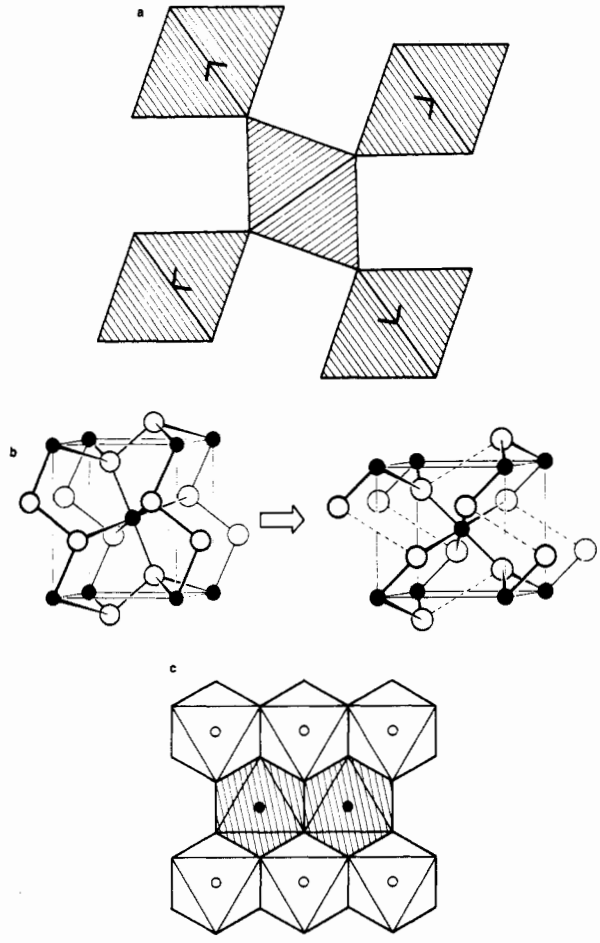

Figure 7. (a) Drawing of the structure of rutile (TiO_2) seen down the infinite chains of edge-sharing octahedra. Comparison with Figure 5b shows how rutile can be derived from marcasite by breaking the dimer bonds. (b) Spoke drawing showing this same derivation (adapted from ref 2). (c) Idealized view of the rutile structure from a direction perpendicular to the edge-sharing chains. Shaded octahedra are occupied at height $x = {}^1/_2$, and unshaded ones at height $x = 0$. In this idealization, the anions at the octahedral vertices form a hexagonal close-packing.

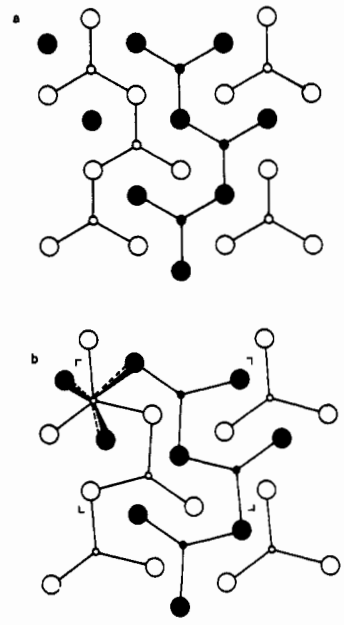

Figure 8. (a) Idealization of the $PbCl_2$ structure. Large circles represent Cl atoms and small circles, Pb. Filled circles are at height ${}^1/_2$ and open ones at height 0. In this structure as in the rutile structure of Figure 7c, from which it is derived, the anions are hexagonally close packed. Here, however, metal–anion bonds have been broken so that the metal atoms have moved to the centers of the faces of their coordination octahedra in rutile. They are therefore coplanar with the anions and are three-coordinate. (b) Observed $PbCl_2$ structure. As shown by the Pb atom at the upper left, the anion framework has distorted so that the lead atoms are roughly nine-coordinate instead of three-coordinate. The coordination polyhedron is a distorted tricapped trigonal prism.

all the dimers are dissociated. Further, the $PbCl_2$ structure (Figure 8) can be regarded as an 18-electron derivative of rutile in which M–X bonds are broken by moving M atoms to the middle of the faces of the MX_6 coordination octahedra.

Yet again, all the dimers in CaC_2 may rotate to the parallel arrangement shown in Figure 9. This type is unknown, but the structures of $CuGaO_2$ and $NaHF_2$ are related to it by inserting spacer atoms of Cu and H, respectively, in the centers of the dimers. If one counts electrons by replacing three-center four-electron bonds at the spacers by two-center two-electron bonds with the spacer atoms deleted, these are also 14-electron compounds. The 16-electron type derived from the 14-electron type in Figure 9 by breaking the dimers is the CdI_2 type (Figure 10). These structural relationships are summarized in Figure 11.

In describing structures as 10-, 14-, or 16-electron types, we have ignored the fact that there are compounds like $CoTe_2$ which occur in both marcasite (14 e) and CdI_2 (16 e) modifications. In these two geometries the cobalt is formally Co^{II} and Co^{IV}, respectively. There are also cases like MnO_2 (16 e) and MnS_2 (14 e), where the number of electrons assigned to a compound in this way can be determined only by knowing its structure. Does this classification therefore have any meaning?

Figure 12 shows the structures of all MX_2 compounds (X = O, S, Se, or Te) having the CaF_2, rutile, CdI_2, pyrite, marcasite, or CaC_2 types as a function of the sum of the third and fourth ionization potentials of M, if those potentials are known.[3] It shows, as one might expect, that metals whose third and fourth ionization potentials are small form 16-electron MX_2 structures, while those with large IP's hold onto these electrons and form 14-electron structures. Further, the more electronegative X, the higher is the sum of IP's needed to obtain a 14-electron structure. There are some anomalous tellurides in this plot, and the dioxides of Ca, Sr, K, and Rb have the 10-e CaC_2 structure for reasons difficult to assess exactly but probably related to the electrostatic energies of these extremely ionic compounds, which may not be well modeled by our molecular orbital, covalent approach. The overall trends, however, suggest that the number of valence electrons ascribed to each of these structure types is in fact of some significance. This should not be taken to imply that the actual charges on the metal atoms in 14- and 16-electron compounds are +2 and +4, respectively, which is almost certainly false. More likely the actual charges are much lower and the filled bands have considerable metal character. Nevertheless, it is interesting that there should be so close an association between ionization potentials and formal charges and the observed structure types.

In what follows, we shall concentrate on the 14-electron structures. It will be shown that the dimer tilting as one moves from 10 to 14 electrons is predicted by extended Hückel calculations and has at its origin the same orbital explanation as the bending of the molecules **1**–**3** discussed above. Simple molecular orbital ideals also enable one to understand why the specific dimer-tilting modes in the observed structures are energetically favorable and to predict how these structures

(3) Huheey, J. E. "Inorganic Chemistry", 2nd ed.; Harper and Row: New York, 1978.

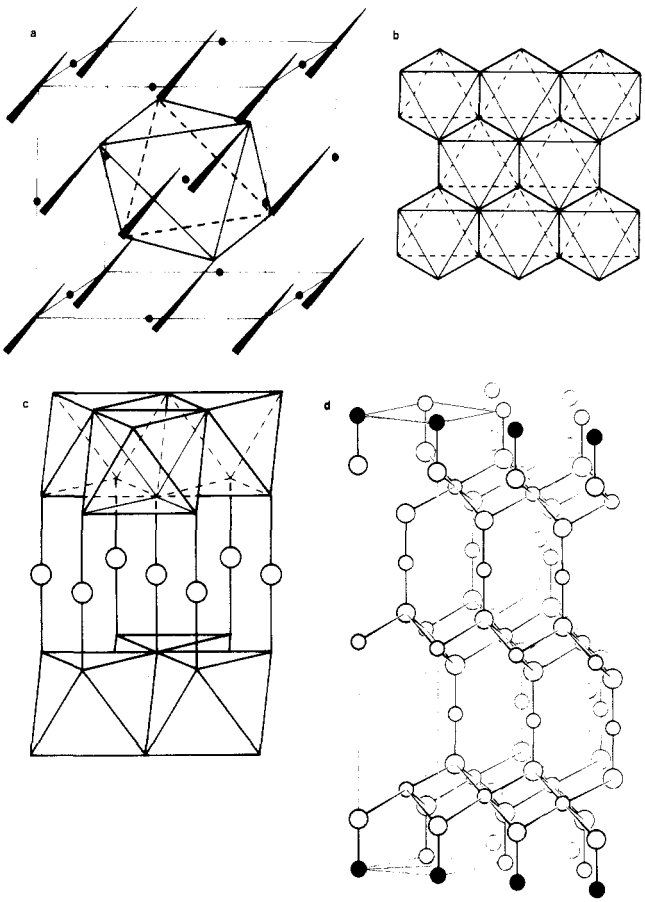

Figure 9. (a) Drawing of the $NaHF_2$ structure, with the conventions of Figure 2 except that in $NaHF_2$ itself dimers are replaced by "isoelectronic" F–H–F trimers. The metal coordination octahedra fuse into the infinite edge-sharing sheets shown in (b), which are linked through F–H–F bonds as shown in (c). (d) Spoke drawing of the same structure, adapted from ref 2.

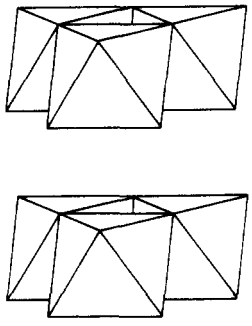

Figure 10. CdI_2 structure derived from that of $NaHF_2$ by breaking the "dimer" bonds. It consists of the octahedral sheets of Figure 9b stacked directly above one another, as shown here.

might distort. As discussed above, we shall use these calculations only as a basis for developing a qualitative understanding that may be applicable to a broad range of compounds, rather than attempting precise computations on a single composition as in ref 4–6.

Dimer Tilting

In order to understand the rotation of the dimers on moving from CaC_2 (10 e) to FeS_2 (14 e), let us first consider the

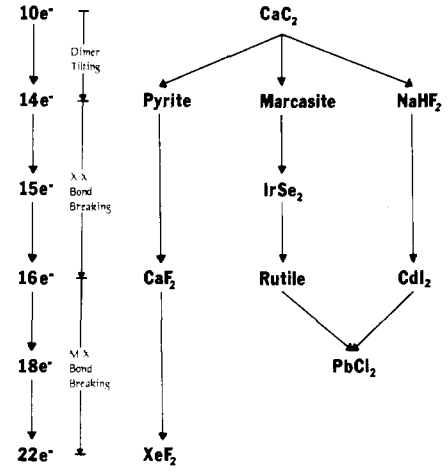

Figure 11. Structural relations among the descendants of CaC_2.

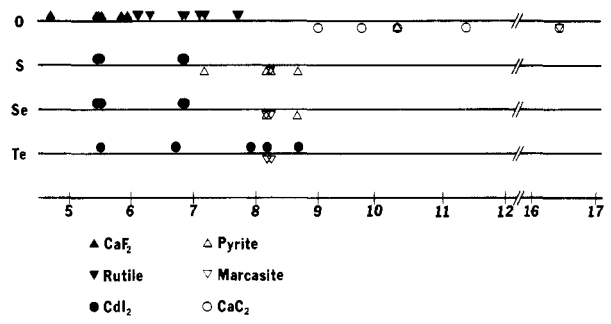

Figure 12. Structures of dioxides and other dichalcogenides as a function of the sum of the third and fourth ionization potentials of the metal atom (in MJ/mol). Structures with 16 electrons are shown by solid symbols lying above the line associated with each anion, and 14- or 10-electron structures by empty symbols lying below the line. Only about one-third of the known compounds with the structures in question are plotted because of the apparent lack of data on higher IP's of nearly all second- and third-row transition metals.

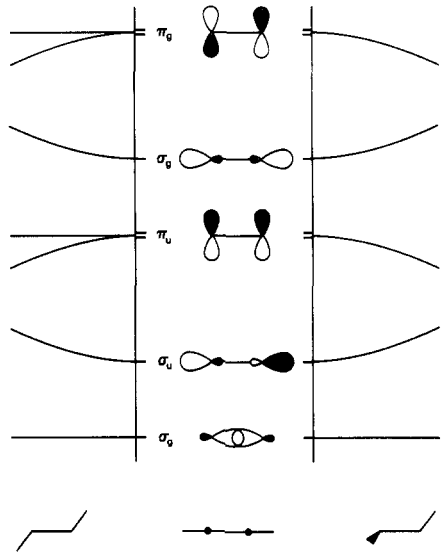

Figure 13. Schematic molecular orbital diagram for an XAAX molecule showing the effect of in-plane (left) and out-of-plane (right) bending on the low-lying orbitals, which are primarily located on the central A_2 dimer.

analogous change in geometry from C_2H_2 (10 e) to O_2H_2 (14 e). This can be rationalized as shown in Figure 13, which depicts schematically the energetic effect of bending an XAAX molecule.[7] Because the ligand (X) orbitals lie above the dimer

(4) Kahn, M. A. *J. Phys. C* **1976**, *9*, 81.
(5) Zunger, A.; Freeman, A. J. *Phys. Rev. B: Solid State* **1977**, *16*, 906.
(6) McCanny, J. V. *J. Phys. C* **1979**, *12*, 3263.

(A_2) orbitals, they mix in a bonding way into the molecular orbitals of the latter. Thus, on bending, dimer orbitals whose overlap with the ligands increases on distortion will drop in energy, while those overlap with the ligands decreases will rise. Extended Hückel calculations support this simple picture.[7] For 10-electron systems, which are occupied through $2\sigma_g$, bending is energetically unfavorable, while for 14-electron molecules, where both π_g levels are filled, it results in a lowering of the overall energy. Planar geometries are found for both isomers (cis and trans) of the "12-electron species" N_2F_2, but O_2F_2 and O_2H_2 are found in the skewed nonplanar arrangement. The factors favoring the nonplanar over the planar structure for the 14-electron O_2H_2 case are discussed elsewhere.[7]

One might expect a similar explanation to apply to the dimer tilting in $CaC_2 \rightarrow FeS_2$, since the occupied orbitals of these compounds are primarily dimer located and the cations are in positions similar to the hydrogens or X atoms above. The simplest way to test this is to consider the tetraatomic unit shown in **6**. In a crystal of CaC_2 or FeS_2, atoms 1 and 4 will

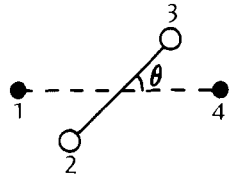

6

be related by a translational symmetry. If we assume the crystal wave function has this same symmetry, then using the language of the extended Hückel approach we can electronically mimic the crystal environment by considering only atoms 1, 2, and 3 but adding S_{ij} and H_{ij} to $S_{ij'}$ and $H_{ij'}$, where i and j are any orbitals on atoms 3 and 4, respectively, and j' is the orbital on 1 corresponding to j on 4. Atom 3 thus feels an interaction with atom 4, but atoms 1 and 4 have been identified, producing a triatomic "crystal" which might be likened to a snake biting its own tail. We have described this process elsewhere.[8] Calculations on this unit by using the Fe and S parameters listed in Appendix 1 produce a level ordering and angular behavior exactly like that of Figure 13. Thus, insofar as the essential features of bonding in the crystal are dictated by this sort of triatomic unit, we would expect 10-electron compounds like CaC_2 to have $\theta = 0°$ and 14-electron compounds like pyrite to have $\theta > 0°$, as observed in practice.

Of course, many interactions that are potentially quite important are excluded by considering only three atoms. Further, not every "molecular orbital" of the infinite chain this triatomic unit mimics needs to be totally symmetric under the infinite translation group of that chain. That is, the assumption that atoms 1 and 4 make identical contributions to the wave function is true only for some orbitals. In order to overcome these difficulties and to obtain meaningful total energies for crystals of CaC_2 or FeS_2, we must study the solid-state analogue of the molecular orbital structure and calculate the energy band structure of these materials. Unlike a molecule, an infinite solid does not possess a single set of molecular orbitals and a corresponding total energy. Instead, it has "molecular orbitals" (energy bands) and energies that depend continuously on a vector $\mathbf{k} = (k_1, k_2, k_3)$ ranging over the Brillouin zone, an infinite set of symmetry labels for the irreducible representations of the crystal's infinite translation group. The total energy is the integral of this calculated energy

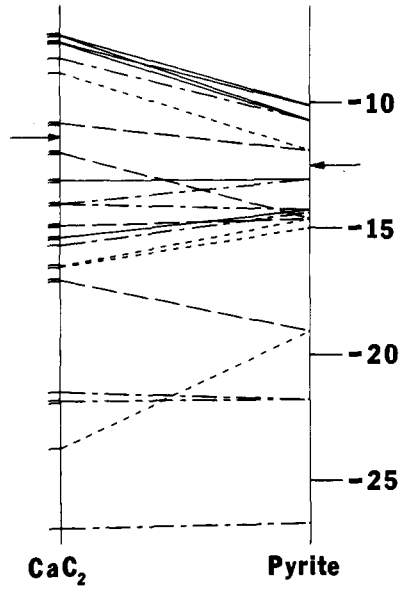

Figure 14. Effects of the rotation of the dimers in FeS_2 from the CaC_2 arrangement to that of pyrite on the low-lying energy bands at $\mathbf{k} = 0$. Only the bands occupied for 14 e/formula unit are shown. The arrows separate filled and vacant orbitals for 10 e/formula unit. Energies are in eV. Solid lines denote π_g orbitals, long dashed lines, π_u orbitals; short dashed lines, σ_u orbitals; and alternating long and short dashed lines, σ_g orbitals. The distinction between σ and π is rigorous only at the CaC_2 structure itself.

over all $\mathbf{k}$. More details of this process may be found in Harrison's books.[9]

The band structure and total energy for a number of structures with varying extents of dimer tilting from $\theta = 0$ (CaC_2) to $\theta = 54°$ (pyrite) were calculated in the extended Hückel approximation by using FeS_2 as a model compound, as outlined in Appendix 1. The geometry chosen for pyrite (FeS_2) was the observed one (see Appendix 1). The other structures had tetragonal unit cells constructed to have the same volume as pyrite and to have the S–S (dimer) distances and the distances between an Fe atom and the two neighboring S atoms above and below it along c for $\theta = 0°$ equal to the values in pyrite. Keeping such bond distances constant is a common practice in simple molecular orbital calculations, due to the sensitivity of the total energy to bond length and the inaccuracy of approximate calculations in predicting correct distances. The constant volume restriction is suggested by experimental results[2b] for KO_2, which is known in both the CaC_2 and NaCl (disordered pyrite) structures, the two differing by only 1.5% in volume. Our basis set consisted only of valence s and p orbitals on all atoms.

The energy bands at $\mathbf{k} = 0$ up through those occupied in pyrite are shown in Figure 14. All of these bands are located primarily on the S_2 units. To aid in the interpretation of this figure, they have been given symmetry labels σ_g, σ_u, π_g, and π_u even though the distinction between σ and π orbitals is rigorous only at $\theta = 0°$. The energy at $\mathbf{k} = 0$ mimics the observed behavior. For 10 electrons per formula unit the CaC_2 type is more stable by 8.4 eV,[10] while for 14 electrons the pyrite type is more stable by 29.4 eV.

The pyrite structure is not the only way of tilting the dimers so that they point along 111 or some equivalent direction. We shall show in a moment that there are eight other structures produced this way with the same size unit cell. If the $\mathbf{k} = 0$

(7) (a) Gimarc, B. M. "Molecular Orbital Structure and Bonding: The Qualitative Molecular Orbital Approach"; Academic Press: New York, 1979. (b) Burdett, J. K.; Albright, T. A. *Inorg. Chem.* **1979**, *18*, 2112.
(8) Burdett, J. K. In "Structure and Bonding in Solids"; O'Keeffe, M., Navrotsky, A., Eds.; Academic Press: New York, 1981.
(9) Harrison, W. A. "Solid State Theory"; Dover Publications: New York, 1979; "Electronic Structure of Solids"; W. H. Freeman: San Francisco, 1980.
(10) Energies of crystals will always refer to one unit cell, not to one formula unit.

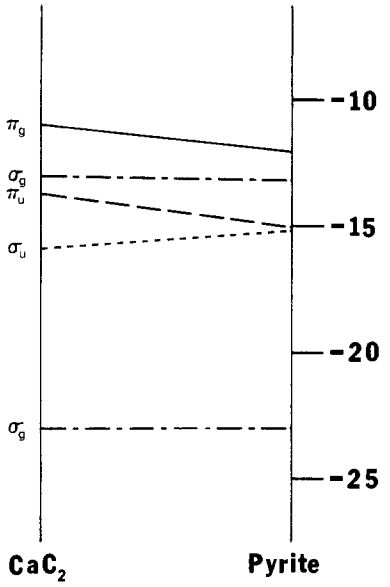

Figure 15. Simplication of Figure 14, produced by averaging the energies of the bands of the same symmetry shown there. The bottom four and top four σ_g levels have been averaged separately. Note the similarity between this figure and Figure 13.

band energies of these structures are also computed, it is found that several of them lie below CaC_2 in energy for 10 electrons, but by no more than 3.4 eV. This is not what would be expected (since it is not apparently in agreement with experiment), but it is not terribly surprising given the well-documented inaccuracy of the extended Hückel approach (or indeed any approximate molecular orbital method) in discriminating among structures with different coordination numbers. In view of this well-known coordination number problem, what is significant about these calculations is not the absolute energies so much as the fact that adding electrons dramatically stabilizes the pyrite relative to the CaC_2 arrangement.

A simplification of Figure 14 can be seen in Figure 15, in which the energies of bands with the same symmetry label have been averaged. Note the strong similarity between this figure and Figure 13, which shows the corresponding levels for the molecular case. Of course, the bands shown here are calculated at only one point in **k** space and may not be totally representative. Further, as Figure 14 shows, the orbitals occupied between 10 and 14 electrons are not all π_g levels, so the detailed picture in the solid state is more complex than that encountered with molecules. Nevertheless it is clear that in the 14-electron crystal as in the "isoelectronic" molecule (O_2H_2) and in the one-dimensional chain described above, the largest driving force favoring pyrite over CaC_2 is the stabilization of the dimer π_g levels on bending.

Structure Enumeration

Having discussed why the S_2 dimers in pyrite tilt away from 001, we now consider why the particular patterns of dimer tilting seen in pyrite, marcasite, and $NaHF_2$ are observed and others are not. In order to do this, it is first necessary to enumerate the probable alternatives to these structures types.

The pyrite unit cell contains four S_2 dimers not related by any translational symmetry. These all point along one of the four symmetry-equivalent directions 111, 11$\bar{1}$, 1$\bar{1}$1, or $\bar{1}$11. The same is true of the distorted marcasite and $NaHF_2$ structures shown in Figures 5 and 9. What other structures exist having the pyrite size unit cell and this dimer orientation?

In principle it might appear that there are $4^4 = 256$ such structures, since each dimer has four possible orientations. This is not the case, since any one of these structures is equivalent to all the other structures obtained from it by the action of some symmetry operation of the space group $Fm3m$ of the NaCl parent. That is, a rotation, translation, or inversion of the pyrite structure shown in Figure 2 still represents pyrite. The group $Fm3m$ thus divides the set of 256 dimer arrangements up into equivalence classes called orbits. To count the distinct structures we must count these group orbits.

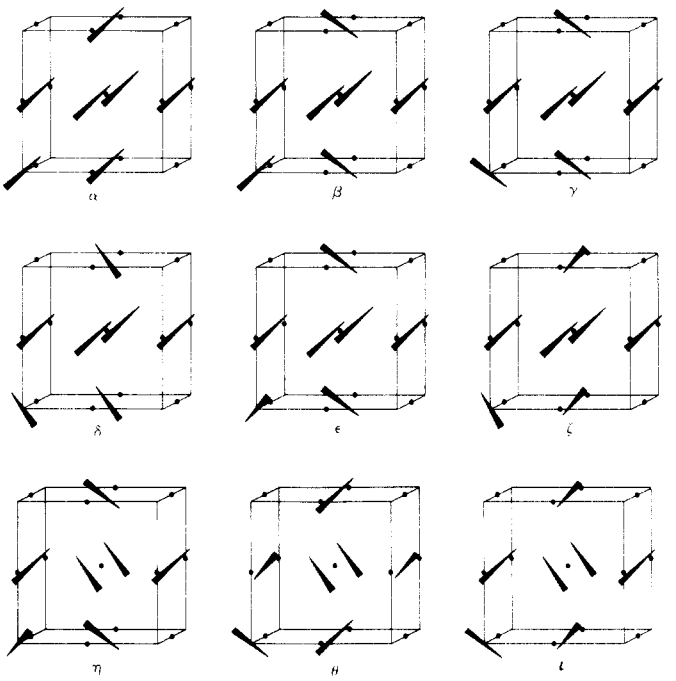

Figure 16. The nine pyrite-like structures with the same size unit cell as pyrite, with the same conventions as in Figure 2. For graphic simplicity, only one of the eight equivalent dimers at the vertices of the unit cell is drawn.

Table I. Band Structure Energies of the Nine Pyrite-like Structures at k = 0 and the Energy $E' = 5.7N_2 + 7.9N_1$ That Approximates It[a]

struct	band E	E'	struct	band E	E'
α	79	69	ζ	74	59
β	60	50	η	0	0
γ	27	23	θ	145	95
δ	67	54	ι	44	32
ϵ	32	27			

[a] Energies are in eV, refer to one unit cell ($Z = 4$), and are computed relative to pyrite = $\eta = 0$. The band energy of pyrite at k = 0 is −844 eV.

This situation in which a set S (the 256 dimer arrrangements) is permuted by a group G and where one wishes to count the G orbits in S can be resolved by using Burnside's lemma.[11] This states that the number, Ω, of orbits is given by the formula $\Omega = |G|^{-1}\sum_{g\in G}\Phi(g)$, where $|G|$ is the order of G and $\Phi(g) = |\{s \in S : gs = s\}|$ is the number of elements S which are fixed by the element g of G, i.e., the number of s having g as a symmetry. This lemma and related results have been used extensively to enumerate both molecular and crystal structures.[1,12]

The use of Burnside's lemma, detailed in Appendix 2, shows that there are nine MX_2 structures having the same size unit cell as pyrite and having the X_2 dimers pointed along 111 or

(11) See, for example: Burnside, W. S. "Theory of Groups of Finite Order", 2nd ed.; Dover Publications: New York, 1955. de Bruijn, N. G. In "Applied Combinatorial Mathematics"; Beckenbach, E. F., Ed.; Wiley: New York, 1964. Harary, F.; Palmer, E. M. "Graphical Enumeration"; Academic Press: New York, 1973. Liu, C. L. "Introduction to Combinatorial Mathematics"; McGraw-Hill: New York, 1968.

(12) For reviews, see: Rouvray, D. H. *Chem. Soc. Rev.* **1974**, *3*, 355. McLarnan, T. J.; Moore, P. B. In "Structure and Bonding in Solids"; O'Keeffe, M., Navrotsky, A., Eds.; Academic Press: New York, 1981.

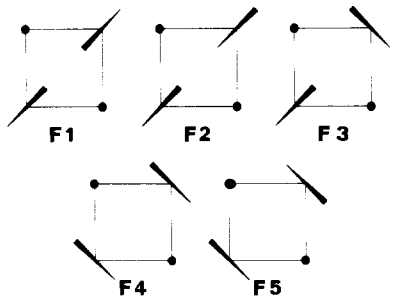

Figure 17. The five possible relative orientations of two nearest neighboring dimers in a pyrite-like structure. The circles are, as usual, metal atoms, and the squares shown are one-half of a unit cell edge in length.

Table II. Extended Hückel Energies and Average Charges on the Iron Atoms in Fragments F1–F5 and the Minimum Distances between the Atoms in the Two S–S Dimers in Those Fragments

fragment	min *d* (S–S nonbonded), Å	*E*, eV	$\langle q_{Fe} \rangle$
F1	2.08	−424.15	0.726
F2	2.42	−426.47	1.529
F3	3.08	−433.75	1.472
F4	3.83	−435.30	1.381
F5	4.03	−435.47	1.365

some equivalent direction. These nine types are shown in Figure 16 and will henceforth be called the pyrite-like structures.

Energies of the Pyrite-like Structures

In order to explore why some of the nine structures occur and others do not, we evaluate their band structure and energy at $\mathbf{k} = 0$ by assuming 14 electrons per formula unit. The results are shown in Table I. These numbers are, of course, only approximations to the properly integrated total energies, but the calculated energy differences are so enormous that errors of a few electron volts in these numbers can easily be tolerated. Calculations at $\mathbf{k} = (1/2, 1/2, 0)$ give similar results, and the calculations reported below on observed structures with use of finer meshes suggests that the mean departures of these energies from the correct averages may be about 10 eV.

To understand these energy differences among the pyrite-like structures, we would like to be able to associate them with some sort of local geometric features. The most obvious difference of this type among these structures is the variation in the nonbonded S–S distance between dimers. The five possible orientations of two nearest neighboring dimers in a pyrite-like structure are shown in Figure 17, and the extended Hückel energies of these six atom fragments are listed in Table II. There is a sharp increase in energy as the nonbonded S–S distance decreases. While the major source of this is certainly S–S repulsion, the metal atoms also play a role, as shown by the variation in the average charge $\langle q_{Fe} \rangle$ on the iron atoms. This stays roughly constant for fragments F2–F5 but drops by nearly one electron charge in F1, whose HOMO is largely of Fe s character. This can be rationalized by observing that with short S–S distance an interdimer antibonding orbital has been pushed to an energy region well above that of the iron 4s orbital. A simpler electron dot picture of what has happened is shown in **7**, which shows the replacement of two nonbonded dimers by a bonded tetramer with a net loss of two electrons to two iron atoms.

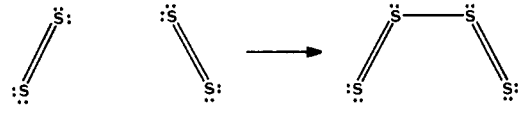

Table III. Band Structure Energies of the Observed Pyrite Structure and Idealized α and γ Structures Having Regular Fe Coordination Octahedra

struct	energy, eV
η = pyrite	−857.6
γ = marcasite	−859.7
α = "$NaHF_2$"	−859.3

The extent of this dimer repulsion in determining the total energy of the nine crystal structures can be assessed by writing an approximate energy $E' = \sum_{i=1}^{5} N_i E(Fi)$, where N_i is the number of contacts of type F*i* found in one unit cell of the structure and $E(Fi)$ is the energy of F*i* from Table II. The geometric constraints of the pyrite-sized unit cell require that $N_1 = N_5$ and $N_2 = N_4$, which allow us to rewrite this as $E' = 5.7N_2 + 7.9N_1$ (eV) relative to $E(F3) = 0$. The results of this calculation, shown in Table I, are in very good agreement with the $\mathbf{k} = 0$ band energy. This means that to a first approximation, the energy differences among these structures are due to dimer–dimer repulsions in an environment containing Fe atoms acting as electron sinks when that repulsion becomes too severe. Repeating the cluster calculations without the Fe atoms results in an additional destabilization of F1 of about 10 eV and a much worse fit to the $\mathbf{k} = 0$ energies, showing that these atoms cannot be ignored. It is not surprising that dimer–dimer repulsions play a major role in determining the total energy, but it is interesting that changes in directional Fe–S bonding as the iron coordination sphere varies from a very flattened trigonal antiprisim (in structure α) to an octahedron (η) to a very elongated trigonal antiprism (θ) seem to be of somewhat secondary importance.

The calculations of Table I correctly predict pyrite (η) to be the most stable of the nine structures. Marcasite (γ) is the second lowest in energy, but $NaHF_2$ (α) is eighth. Further, even marcasite lies about 27 eV/unit cell, or about 150 kcal/formula unit, above pyrite. The reason for this is that the model geometries of the α and γ types both differ substantially from those observed in having very distorted Fe coordination octahedra. In order to assess the energies of these types more accurately, we therefore repeated the band structure calculations using model geometries having regular octahedral coordination at Fe with the same S–S (dimer) and Fe–S distances used above. These are not precisely the observed atomic arrangements, but are much closer approximations than the earlier models. Band structure calculations were performed at the special points $\mathbf{k} = (k_1, k_2, k_3)$ where $k_i = \pm 1/8$ or $\pm 3/8$, as described ref 2a and 13, and the energies at these points were averaged to obtain a more accurate integrated total energy. The results in Table III show that the α and γ structures in fact dropped below the energy of the η structure (pyrite), though not by a disturbing amount given the approximate nature of our approach.

It is interesting to note in this regard that structural sorting maps of the kind applied to MX_2 compounds by Mooser and Pearson[14] and Burdett et al.,[15] which are designed to produce two-dimensional plots in which compounds with different structure types occupy different regions of the plane, fail to separate the pyrite and marcasite types. This suggests—though it by no means proves—that the energetic reasons for the choice of one or the other of these two structures may be rather subtle.

The calculations on pyrite, marcasite, and $NaHF_2$ suggest that some of the other pyrite-like structures might be able to undergo distortions that would bring them close to pyrite in

(13) (a) Baldereschi, A. *Phys. Rev. B* **1973**, *7*, 5212. (b) Chadi, D. J.; Cohen, M. L. *Ibid.* **1973**, *8*, 5747.
(14) Mooser, E.; Pearson, W. B. Acta Crystallogr. **1959**, *12*, 1015.
(15) Burdett, J. K.; Price, G. D.; Price, S. L. *Phys. Rev. B* **1981**, *24*, 2903.

energy. Such distortions would require large dimer–dimer separations and thus nearly regular octahedral coordination of Fe. To see whether such distortions are possible, we used Villiger's[16] DLS program, which varies atomic coordinates and cell constants to provide the best possible weighted least-squares fit of a given set of interatomic distances to prescribed values. The Fe–S and S–S (dimer) distances were prescribed to be those of pyrite, and the S–S (nonbonded) distances were those which would make the iron coordination octahedron regular. Geometries and band energies were computed for the ϵ structure by using weights w(Fe–S) = w(S–S (dimer)) = 1 and w(S–S (nonbonded)) ranging from 0.1 to 1. The weight of S–S (nonbonded) had a effect on the final DLS geometry but a small effect on the energy at $\mathbf{k} = 0$, which dropped from 32 to 18 eV relative to pyrite, but no lower. Because of this, a weight of 0.4 (which seemed to give the most plausible variations in distance) was used for the other pyrite-like structures. The β structure dropped in energy from 60 to 13 eV in this calculation, and distortions of all other structures led to some very short (and unrealistic) interatomic distances, which caused the band structure program to fail. They would lie very high in energy. Thus, no structure except for the three observed types appears to be capable of distorting to produce a regular geometry with a low total energy, and we predict that none of these other types should be found.

For reasons of computational economy, none of these calculations have included d orbitals on the metal atoms. Including d orbitals and repeating the calculations where feasible (i.e., where the number of orbitals in the unit cell is not too large) produce more complicated but qualitatively similar results (see Appendix 1). This contrasts with the situation in the following section, where d orbitals are quite important.

Löllingite Distortion

Finally, we consider what can be said about the distortions away from a regular octahedral geometry that are found in the observed structures. The most striking of these is that observed in löllingite ($FeAs_2$), which has the marcasite structure with a sizable compresson along c, the direction of the edge-sharing chains of octahedra. The effect on the iron coordination octahedron is shown in **8**. The magnitude of this

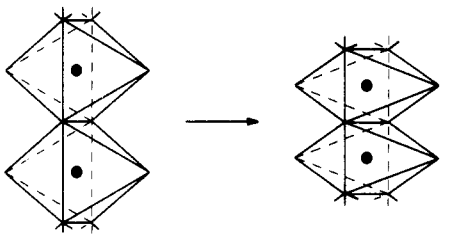

8

distortion can be seen in the ratio of c/a, which is 0.762 in marcasite and 0.544 in löllingite.

The origins of the löllingite distortion are not obvious. It is not the case, for example, that all compounds with 14 s and p valence electrons have the marcasite structure and all 12-electron compounds have the löllingite type. In particular, while the dipnictides of Fe, Ru, and Os have the löllingite structure, $NiAs_2$ and $NiSb_2$ have the marcasite type. It is, however, the case that d^2 and d^4 compounds take the löllingite structure while d^6 and d^7 compounds are marcasites.[17] Compounds like $CoAs_2$ with five d electrons have a structure with a doubled c axis and alternating long and short Co–Co distances along c.[18] Although there is a slight distortion to monoclinic geometry, the intermediate $c/a = 2 \times 0.60$ ratio is still meaningful. Further, in the solid solution among $FeAs_2$ (d^4), $CoAs_2$ (d^5), and $NiAs_2$ (d^6), the structural parameters vary continously as functions of the number of d electrons.[19] Finally, the electronic structure and properties of these materials depend on more subtle effects still: $NiAs_2$ is a semiconductor, while $NiSb_2$, with an identical c/a ratio, is a metal.[17] This is a particular problem, since our procedure for computing the total energy of a crystal via the special points method requires modification to apply to metals, which have partially filled bands.

In short, a simple qualitative explanation for the löllingite distortion is perhaps to much to ask for. Nevertheless, we can use extended Hückel band structure calculations as a "black box" and see whether they predict this distortion. We consider three model structures: an ideal marcasite having the FeS_6 octahedra regular and possessing a c/a ratio of 0.681; a stretched marcasite with $c/a = 0.750$, which more nearly approximates the observed structures; and a löllingite with $c/a = 0.533$. All these structures have the same bonded S–S and Fe–S distances we have used above; there is a decrease in volume of approximately 9% from the stretched structure to the löllingite.

Calculation of the total energies of these structures by using the s–p valence basis set employed above produces the result that for both 12- and 14-electron compounds the löllingite structure is about 5 eV less stable than the ideal and stretched marcasite structures, which lie close together in energy. Further, all three structures with 12 valence electrons are calculated to be metals, in contrast with the observation that the known compounds with the löllingite structure are semiconductors. This bears out our expectation that s and p orbitals alone do not suffice to explain the löllingite distortion.

Inclusion of d orbitals on Fe, however, improves the results substantially. If the total energies are computed by averaging the energies at the special points[2a] (k_1, k_2, k_3), $k_i = \pm^1/_8$ or $\pm^3/_8$, then for the d^6 case the löllingite structure again lies about 5 eV above the two marcasite structures, but for the d^4 case the löllingite modification lies a few tenths of an eV below the ideal marcasite and about 1 eV below the stretched marcasite. While these energy differences are somewhat uncertain because the variation in energy with $\mathbf{k}$ is large and because the unobserved structures are metallic (but just barely), they nevertheless tend in the right direction. Further, all observed structures are correctly predicted to be semiconductors. Unfortunately, in the d^2 and d^7 cases all three structures are predicted (incorrectly) to be metals, and we can say nothing about which type will be preferred. In addition, the substantial variation in energy in both marcasite and löllingite as a function of $\mathbf{k}$ means that it is difficult to give a simple explanation of the results of these calculations. For either d^4 or d^6 there are regions of $\mathbf{k}$ space where the energy of marcasite is lower than that of löllingite and regions where löllingite lies below marcasite; only the integrated total energy shows the correct behavior. The character of the occupied orbitals also changes as a function of $\mathbf{k}$, which makes it impossible to determine the exact occupancy of the d levels or the charge on the dimers. Thus, we cannot directly address the interpretation Tossell et al.[20] have given to these structures, which relies on these quantities. The complexity of the calculations including d orbitals and the failure of those omitting such orbitals suggest, however, that an explanation based on dimer charges is telling only part of the story.

(16) Villiger, H. "DLS-Manual"; ETH: Zurich, 1975.
(17) Pearson, W. B. *Z. Kristallogr., Kristallgeom., Kristallphys.* **1965**, *121*, 449.
(18) Zhdanov, G. S.; Kuz'min, R. N., *Sov. Phys.—Crystallogr. (Engl. Transl.)* **1962**, *6*, 704.
(19) Roseboom, E. H., Jr. *Am. Mineral.* **1963**, *48*, 271.
(20) Tossell, J. A.; Vaughan, D. J.; Burdett, J. K. *Phys. Chem. Miner.* **1981**, *7*, 177.

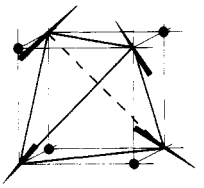

Figure 18. One-eight of a unit cell of a pyrite-like structure (pyrite itself in this case), showing how the centers of the four nonequivalent dimers sit at the vertices of a tetrahedron whose center is at $^1/_4$, $^1/_4$, $^1/_4$.

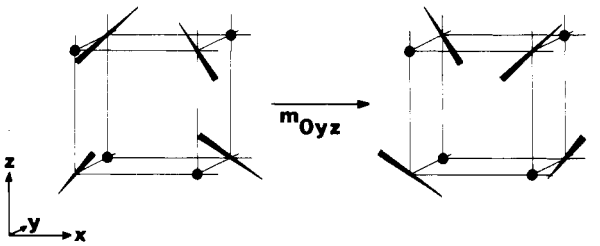

Figure 19. Effect of the mirror at 0, y, z (m_{0yz} or m_{100}) on the four inequivalent dimers in pyrite. This mirror operation is not a symmetry of pyrite, but it does produce an equivalent structure, i.e., a pyrite cell in a different orientation or position.

Table IV. Use of Burnside's Lemma To Count Possible MX_2 Structures with the Pyrite Unit Cell Having X_2 Dimers Oriented along 111 or Some Equivalent Direction[a]

g	no. of g	$\Phi(g)$
1	1	256
3_{111}	8	4
$\bar{4}_{100}$	6	4
2_{100}	3	16
m_{110}	6	16
m_{100}	3	0
$3_{111}\cdot m_{100}$	24	4
$\bar{4}_{100}\cdot m_{100}$	6	4
$\bar{4}_{100}\cdot m_{010}$	12	4
$2_{100}\cdot m_{100}$	3	16
$2_{100}\cdot m_{010}$	6	16
$m_{110}\cdot m_{100}$	12	0
$m_{110}\cdot m_{001}$	6	16
total	96	864

[a] The left column lists representative elements of $Fm3m/P\bar{1}$. The first five elements are class representatives of $\bar{4}3m$ at $^1/_4$, $^1/_4$, $^1/_4$. The element m_{100} is the mirror at 0, y, z and the later elements are symmetries in $\bar{4}3m$ followed by reflections in such mirrors. The second column lists the number of elements of $Fm3m/P\bar{1}$ obtained by a similar geometric construction. For example, there are three elements of $Fm3m/P\bar{1}$ obtained by following a 2-fold axis in $\bar{4}3m$ by a perpendicular mirror through 0, 0, 0 and six elements obtained by following a 2-fold axis by a parallel mirror. The elements grouped together in this table are all conjugate, but the conjugacy classes may be larger than the sets shown here. For example, $3_{111} \sim 3_{111}\cdot m_{100}$. The last column shows the number of dimer arrangements invariant under the given operation. By Burnside's lemma, the number of possible structures is 864/96 = 9.

Despite all these complications, it is pleasing that even in dealing with properties as subtle as the löllingite distortion, extended Hückel band structure calculations predict the correct structures in the two cases, d^4 and d^6, they are able to address.

Summary

The extended Hückel method is thus able to describe the observed tilting of the dimers as electrons are added to the 10-electron CaC_2 structure in a way analogous to the explanation it provides for the corresponding case in A_2X_2 molecules. It further rationalizes the direction of this tilting by showing that of the nine possible structures produced in this way, the three observed ones lie lowest in energy. The energies calculated for these structures are compatible with the energies of finite model clusters. Finally, this method predicts that the cell compression found in löllingite should be favored by d^4 and not by d^6 metals.

Evidence is thus accumulating to suggest that the factors influencing bonding in molecules and solids are indeed quite similar. Moreover, the qualitative and quantitative understanding that simple molecular orbital ideas have given us of isolated small molecules is a productive basis on which to build our ideas of the infinite molecules of the solid state.

Acknowledgment. We thank the donors of the Petroleum Research Fund, administered by the American Chemical Society, for their partial support of this research. We are also grateful to the National Science Foundation for their support under NSF Grant DMR 8019741.

Appendix 1. Computational Details

Band structure calculations were performed by using the extended Hückel method by a program written by Whangbo,[21] whose aid in supplying this program is most gratefully acknowledged. Energies were calculated either at $\mathbf{k} = 0$ or at the special points (k_1, k_2, k_3), where $k_i = \pm^1/_8$ or $\pm^3/_8$, which provide a better approximation to the properly integrated total energy.[2a] A general discussion of the special points method can be found in the references in ref 13.

The atomic parameters employed were for S $H_{ii}(3s) = -20.0$ eV, $H_{ii}(3p) = -13.3$ eV, Slater exponent = 1.817, and for Fe $H_{ii}(4s) = -9.0$ eV, $H_{ii}(4p) = -4.5$ eV, Slater exponent = 0.950. Some of the calculations on the löllingite distortion were repeated with a different set of Fe parameters due to Hoffmann et al.:[22] $H_{ii}(4s) = -9.99$ eV; $H_{ii}(4p) = -5.97$ eV; a Slater exponent of 1.90. The results were qualitatively identical with those where the other choice of Fe parameters was used. Calculations on marcasite and löllingite including d orbitals used these Fe 4s and 4p parameters and had $H_{ii}(3d) = -12.63$ eV with a Slater exponent of 2.50.

Calculations including iron 3d orbitals on crystal structures α, γ, and δ and on the marcasite and $NaHF_2$ structures with regular octahedral coordination at Fe are somewhat parameter sensitive. All reasonable parameter choices result in the structures with regular coordination being more stable for the range d^4–d^{10}, which includes the observed compounds except for $CrSb_2$, a d^2 löllingite type with a quite distorted metal coordination. For d^6–d^{10} the regular structures are much more stable. With more contracted Fe 4s and 4p orbitals or with higher energy 3d orbitals, this range expands to include smaller numbers of d electrons, and the calculations on fragments F1–F5 begin to resemble those reported in the text. In all cases, inclusion of d orbitals decreases the energy differences between regular and distorted structures by a factor of a third to a half, presumably because the energy at which electrons can move from the S_2 dimers to the metal atoms is lower. Thus, despite an increase (considerable) in complexity, the qualitative results do not change dramatically.

The geometric parameters used for pyrite were $c = 5.42$ Å $u = 0.386$, which result in an Fe–S distance of 2.2673 Å and an S–S distance of 2.1404 Å, which we used where relevant in other model crystal and molecular structures.

Appendix 2. Details of Structure Enumeration

In order to apply Burnside's lemma to the problem of counting pyrite-like structures, we must first replace the infinite space group $Fm3m$ with a finite group including the same permutations of the set S of the 256 dimer arrangements.

(21) Whangbo, M. H.; Hoffmann, R. J. *J. Am. Chem. Soc.* **1978**, *100*, 6093. Whangbo, M. H. *Inorg. Chem.* **1980**, *19*, 1723.
(22) Hoffmann, R.; Chen, M. M.-L.; Thorn, D. L. *Inorg. Chem.* **1977**, *16*, 503.

Each of these arrangements is fixed by the primitive cell translations of the pyrite cell and by the inversion centers at the Fe atoms and the midpoints of the dimers. Hence every element of the normal subgroup $P\bar{1}$ of $Fm3m$ corresponds to the identity permutation on S. The distinct permutations of S engendered by $Fm3m$ are therefore represented by the elements of the quotient group $Fm3m/P\bar{1}$ of order 96. The elements of this group are the cosets represented by the 24 elements of the point group $\bar{4}3m = T_d$ of the point $^1/_4$, $^1/_4$, $^1/_4$ of the NaCl cell and the 72 operations obtained by following these 24 by a reflection in one of the mirrors at x, y, 0; x, 0, z, or 0, y, z.

The set S can also be simplified a bit. The centers of the four translationally inequivalent dimers are at the vertices of a tetrahedron centered at $^1/_4$, $^1/_4$, $^1/_4$ (Figure 18). Hence S can be regarded as the set of all 256 ways to place at each vertex of this tetrahedron a dimer parallel to one of the four 3-fold axes of the tetrahedron (not necessarily the 3-fold axis passing through that vertex). The elements of $\bar{4}3m$ permute these objects in the obvious way, and the mirror planes act on them as shown in Figure 19.

To determine $\Phi(g)$ for every $g \in Fm3m/P\bar{1}$ is not as difficult as might at first appear. In particular, it is not necessary to consider all 256 elements of S. Consider, for example, how to evaluate $\Phi(3)$, the number of elements of S fixed by a 3-fold rotor in $\bar{4}3m$. Plainly the dimer on the apical vertex—that through which the rotor passes—of such an element of S must point along that 3-fold axis. The basal dimers need not have this orientation, but once one basal dimer has been specified, the 3-fold symmetry determines the orientations of the others. Thus $\Phi(3) = 4$. This type of consideration makes determination of $\Phi(g)$ for any g fairly easy. It is also extremely helpful that $\Phi(g)$ is a class function.

Table IV lists the value of $\Phi(g)$ for every $g \in Fm3m/P\bar{1}$. Summation of these and division by 96, the order of $Fm3m/P\bar{1}$, produce the answer that there are nine orbits, i.e., nine structures with the same size unit cell as pyrite and with dimers pointing along $\pm1\pm1\pm1$.

Registry No. Pyrite, 1309-36-0; marcasite, 1317-66-4; $NaHF_2$, 1333-83-1; CaC_2, 75-20-7; CaF_2, 7789-75-5; XeF_2, 13709-36-9; $IrSe_2$, 12030-55-6; TiO_2, 13463-67-7; $PbCl_2$, 7758-95-4; CdI_2, 7790-80-9; löllingite, 12255-65-1; $FeAs_2$, 12006-21-2; FeS_2, 12068-85-8.

Contribution from the Baker Laboratory of Chemistry, Cornell University, Ithaca, New York 14853, and Institut für Physikalische Chemie, Universität Wien, A-1090 Wien, Austria

Structural Chemistry and Magnetic Properties of the Compounds $EuOs_4B_4$ and $EuIr_4B_4$ and of the Solid Solutions $(RE)Os_4B_4$-$(RE)Ir_4B_4$ (RE = Ce, Pr, Sm)

KURT HIEBL, PETER ROGL, and M. J. SIENKO*

Received August 18, 1981

New ternary metal borides, $EuOs_4B_4$ and $EuIr_4B_4$, have been synthesized from the elements. The compounds were found to crystallize with the structure type of $NdCo_4B_4$. Effective paramagnetic moments derived from χ^{-1} vs. T plots over the range 1.8–800 K are in good agreement with theoretical values according to a Hund's rule ground-state $^8S_{1/2}$ for a free Eu^{2+} ion. Complete solid solution was found for mixed crystals of $CeOs_4B_4$–$CeIr_4B_4$ (arc melted, quenched, $NdCo_4B_4$-type structure) revealing a positive deviation from Vegard's law. Magnetic susceptibilities were determined for the temperature range 1.8–1000 K. At high temperature the magnetic properties are characterized by Van Vleck paramagnetism of closely spaced multiplets due to admixture of the excited term $J = {}^7/_2$ of the Ce^{3+} $F_{5/2}$ ground state. At lower temperatures the paramagnetic behavior of cerium changes from that of a practically pure Ce^{4+} state in $CeOs_4B_4$ ($\mu_{eff} = 0.49\ \mu_B$) to that of a pronounced Ce^{3+} state in $CeIr_4B_4$ ($\mu_{eff} = 2.21\ \mu_B$) presumably due to the larger iridium metal framework and/or the higher electron-to-atom ratio. At very low temperatures, ≤3.5 K, ferromagnetic ordering was observed for $CeIr_4B_4$ and $CeIr_3Os_1B_4$. For comparison, the magnetic behavior was studied over the range 1.5–300 K of the pseudobinary sections $PrOs_{4-x}Ir_xB_4$ and $SmOs_{4-x}Ir_xB_4$. Although a slight negative deviation from Vegard's law was observed, there was practically no change from a valence state of Sm^{3+} for samarium. On the basis of Miedema's model, a thermodynamic calculation for the valence change ($Ce^{III} \rightarrow Ce^{IV}$, $Eu^{II} \rightarrow Eu^{III}$) has been found to be in good accord with the magnetic behavior observed.

Introduction

Recently published papers[1-3] have shown that 1:4:4 combinations of large rare-earth (RE) metals (La to Gd) with noble metals of highest density (Os and Ir) and boron commonly adopt the $NdCo_4B_4$ type of structure. No data, however, were provided for the corresponding europium compounds due to the extremely high vapor pressure of europium metal at elevated temperatures, which demands more special reaction techniques. So far as crystal chemistry is concerned, following the general behavior of the $RE[Os,Ir]_4B_4$ series of compounds for large RE members, europium was expected to form $NdCo_4B_4$-type analogues in both cases: $EuOs_4B_4$ and $EuIr_4B_4$. Thus, a careful investigation with respect to compound formation and crystal structure, as well as magnetic and superconducting properties, became the subject of the present work.

Second, we have undertaken a detailed study of the crystal chemistry and magnetic properties within the series of solid solutions of mixed crystals $CeOs_{4-x}Ir_xB_4$, $PrOs_{4-x}Ir_xB_4$, and $SmOs_{4-x}Ir_xB_4$, especially in relation to possible intermediate valence behavior of the rare-earth atoms.

Experimental Section

All the compounds were made from commercially available high-purity materials: crystalline boron, 99.7%, from Ventron GmbH, Karlsruhe, Federal Republic of Germany; Os, Ir powders, 99.9%, Degussa, Hanau, Federal Republic of Germany; RE metal ingots, m3N, Ventron GmbH; EuB_6 powder (≤100 ppm, a = 4.1852 Å), Electroschmelzwerk Kempten, Federal Republic of Germany. Powders of the elements and filings of the RE metals wre compacted in steel dies without the use of binders or lubricants. Sample preparation was different for europium and [Ce, Pr, Sm]-containing specimens. (a) The [Ce, Pr, Sm]-containing pellets (~1 g) were arc melted on a water-cooled copper hearth, with use of a nonconsumable tungsten

* To whom correspondence should be addressed at Cornell University.

(1) Rogl, P. *Monatsh. Chem.* **1979**, *110*, 235.
(2) Rogl, P. *Monatsh. Chem.* **1980**, *111*, 517.
(3) Rogl, P.; Nowotny, H. In "The Rare Earths in Modern Science and Technology"; McCarthy, G. J., Rhyne, J. J., Silber, H. B., Eds.; Plenum Press: New York, 1980; Vol. 2, p 173.

0020-1669/82/1321-1128$01.25/0